Argonaute 2 immunoprecipitation revealed large tumor suppressor kinase 1 as a novel proapoptotic target of miR-21 in T cells

Teteloshvili, Nato; Smigielska-Czepiel, Katarzyna; Yuan, Ye; Seitz, Annika; de Jong, Debora; Rutgers, Bea; Jellema, Pytrick; van der Lei, Roelof Jan; Slezak-Prochazka, Izabella; Brouwer, Elisabeth

Published in:
Febs Journal

DOI:
10.1111/febs.14011

Publication date:
2017

The FEBS Journal

FEBS PRESS science publishing by scientists

EDITOR'S CHOICE

Argonaute 2 immunoprecipitation revealed large tumor suppressor kinase 1 as a novel proapoptotic target of miR-21 in T cells

Nato Teteloshvili[1,2,*,#], Katarzyna Smigielska-Czepiel[1,2,#], Ye Yuan[1,3], Annika Seitz[1], Debora de Jong[1], Bea Rutgers[1], Pytrick Jellema[1], Roelof Jan van der Lei[1], Izabella Slezak-Prochazka[1], Elisabeth Brouwer[2,4], Annemieke M.H. Boots[2,4], Bart-Jan Kroesen[2,5], Anke van den Berg[1,2] and Joost Kluiver[1]

1 Department of Pathology and Medical Biology, University of Groningen, University Medical Center Groningen, The Netherlands
2 Groningen Research initiative on healthy Ageing and Immune Longevity (GRAIL), University of Groningen, University Medical Center Groningen, The Netherlands
3 Institute of Clinical Pharmacology of the Second Affiliated Hospital, Harbin Medical University, Heilongjiang Province, China
4 Department of Rheumatology and Clinical Immunology, University of Groningen, University Medical Center Groningen, The Netherlands
5 Department of Laboratory Medicine, University of Groningen, University Medical Center Groningen, The Netherlands

Keywords
AGO2-RIP; apoptosis; LATS1; miR-21; T cells

Correspondence
J. Kluiver, Department of Pathology & Medical Biology, University of Groningen, University Medical Center Groningen, P.O. Box 30.001, 9700 RB Groningen, The Netherlands
Fax: +31-50-3619107
Tel: +31-50-3615788
E-mail: j.l.kluiver@umcg.nl
Website: http://www.rug.nl/staff/j.l.kluiver/

***Present Address**
Department of Medicine, Columbia Center for Translational Immunology, Columbia University Medical Center, New York, USA

#These authors contributed equally.

(Received 30 August 2016, revised 9 December 2016, accepted 9 January 2017)

doi:10.1111/febs.14011

MicroRNA (miR)-21 is an important suppressor of T-cell apoptosis that is also overexpressed in many types of cancers. The exact mechanisms underlying the antiapoptotic effects of miR-21 are not well understood. In this study, we used the Jurkat T-cell line as a model to identify apoptosis-associated miR-21 target genes. We showed that expression of miR-21 rapidly increases upon αCD3/αCD28 activation of Jurkat cells. Inhibition of miR-21 reduced cell growth which could be explained by an increase in apoptosis. MicroRNA target gene identification by AGO2 RNA-immunoprecipitation followed by gene expression microarray (RIP-Chip) resulted in the identification of 72 predicted miR-21 target genes that were at least twofold enriched in the AGO2-IP fraction of miR-21 overexpressing cells. Of these, 71 were at least twofold more enriched in the AGO2-IP fraction of miR-21 overexpressing cells as compared to AGO2-IP fraction of control cells. The target gene for which the AGO2-IP enrichment was most prominently increased upon miR-21 overexpression was the proapoptotic protein LATS1. Luciferase reporter assays and western blot analysis confirmed targeting of LATS1 by miR-21. qRT-PCR analysis in primary T cells showed an inverse expression pattern between LATS1 transcript levels and miR-21 upon T-cell stimulation. Finally, LATS1 knockdown partially rescued the miR-21 inhibition-induced impaired cell growth. Collectively, these data identify LATS1 as a miR-21 target important for the antiapoptotic function of miR-21 in T cells and likely also in many types of cancer.

Introduction

Increased miR-21 levels have been shown in various types of solid tumors as well as in hematological malignancies [1–6]. Consistent with the marked overexpression in cancer, several studies showed an

Abbreviations
LATS1, large tumor suppressor kinase 1; miRNA, microRNA; RIP-Chip, RNA-binding protein immunoprecipitation–microarray profiling.

antiapoptotic effect of miR-21. Knockdown of miR-21 correlates with increased apoptosis and reduced proliferation of breast cancer cells [2,3]. Multiple cancer-relevant miR-21 target genes, such as tropomyosin 1 (TPM1), programmed cell death 4 (PDCD4), phosphatase and tensin homolog (PTEN), Maspin, and SNF-related, matrix-associated, actin-dependent regulator of chromatin, subfamily A, member 4 (SMARCA4), have been identified [4–9]. More recent studies also showed effects of miR-21 on T-cell activation and survival [10–13]. We previously showed that memory T cells are characterized by a high expression of miR-21. In addition, we showed that activation-induced miR-21 provides critical antiapoptotic signals in memory T cells allowing long-term survival [11,14]. However, the miR-21 target genes responsible for the protection against activation-induced apoptosis of T cells remain unknown.

In this study, we set out to investigate miR-21 target genes related to its antiapoptotic effects on T cells. We employed an experimental RNA-immunoprecipitation followed by gene expression microarray (RIP-Chip)-based approach [15] in Jurkat cells. These cells are a commonly used model to study regulatory pathways involved in T-cell activation and apoptosis. We identified the proapoptotic large tumor suppressor kinase 1 (LATS1) as the miR-21 target gene whose enrichment in the argonaute 2 immunoprecipitated (AGO2-IP) increased the most upon miR-21 overexpression and showed its role in the antiapoptotic effect of miR-21.

Results and discussion

Jurkat is a suitable model to study the antiapoptotic role of miR-21

To assess if the Jurkat cell line is a suitable model to study the function of miR-21 in relation to apoptosis, we determined miR-21 expression levels in unstimulated cells and after stimulation with αCD3/αCD28. In comparison to other miRNAs known to be expressed in T cells at high (miR-17) or low (miR-146a) levels, miR-21 levels were moderate in unstimulated cells (Fig. 1A). Activation of Jurkat cells with αCD3/αCD28 for 3 days revealed a marked induction of miR-21 expression (≥25-fold, $P \leq 0.001$; Fig. 1B) consistent with previous studies on αCD3/αCD28-stimulated primary T cells [11,13]. To determine whether loss of miR-21 resulted in a growth defect, we infected Jurkat cells with a miR-21 inhibitor vector which coexpresses GFP. GFP analysis over time of a mixture of transduced and nontransduced cells (GFP competition assay) revealed a significant decrease of miR-21 inhibitor-transduced (GFP-positive) cells when compared to nontransduced (GFP-negative) cells (Fig. 1C). Cells transduced with three nontargeting (NT) control inhibitors showed no effect on cell growth in the GFP competition assay (Fig. 1C and data not shown). Jurkat cells transduced with miR-21 inhibitor showed a significant decrease of viable cells starting at day 4, which was not observed with control transduced cells (Fig. 1D). This effect was paralleled by an increase of apoptotic cells reaching > 80% at day 6 (Fig. 1E,F). These findings are consistent with our reported findings in primary T cells [11] and indicate that endogenous levels of miR-21 in Jurkat cells provide an essential antiapoptotic signal. Together, these data show that the Jurkat cell line is a suitable model to study the antiapoptotic properties of miR-21 in T cells.

miR-21 target genes involved in apoptosis

To identify the antiapoptotic miR-21 target genes, we performed AGO2-RIP-Chip on Jurkat cells overexpressing miR-21 (Jurkat-miR-21) and used cells transduced with an empty vector construct (Jurkat-EV) as a control. The miR-21 levels showed an increase of ~ 22-fold in Jurkat-miR-21 compared to Jurkat-EV (Fig. 2A). Overexpression of miR-21 in Jurkat cells did not cause any obvious effects on the percentage of live cells (data not shown). The efficiency of the AGO2 immunoprecipitation (AGO2-IP) as determined by western blot was comparable between Jurkat-EV and Jurkat-miR-21 cells (Fig. 2B). As expected, miR-21 was strongly enriched in the Jurkat-miR-21 AGO2-IP fraction in comparison to the Jurkat-miR-21 total fraction and the Jurkat-miR-21 and Jurkat-EV IgG1 control IP fractions. Some miR-21 enrichment could also be observed in the Jurkat-EV AGO2-IP fraction as Jurkat cells endogenously express moderate miR-21 levels (Figs. 2C and 1A).

Gene set enrichment analysis (GSEA) [16] revealed a strong enrichment of multiple microRNA (miRNA)-binding motifs in both Jurkat-miR-21 (8 of the top 10) and Jurkat-EV (9 of the top 10, Table 1) further validating the efficiency of the AGO2-RIP. The miR-21-binding motif increased from the 46th position of most enriched gene sets in Jurkat-EV (false discovery rate (FDR) = 0.0013) to the 28th position in Jurkat-miR-21 cells (FDR ≤ 0.001). Comparison of both top-10 enriched gene sets revealed a marked overlap between Jurkat-miR-21 and Jurkat-EV cells with eight shared gene sets (Table 1). A marked difference was observed for two apoptosis-related gene sets. Genes regulated upon treatment with the growth and survival factor, IL-6, were among the top-10 most enriched gene sets in Jurkat-EV but not in Jurkat-miR-21 (position 258).

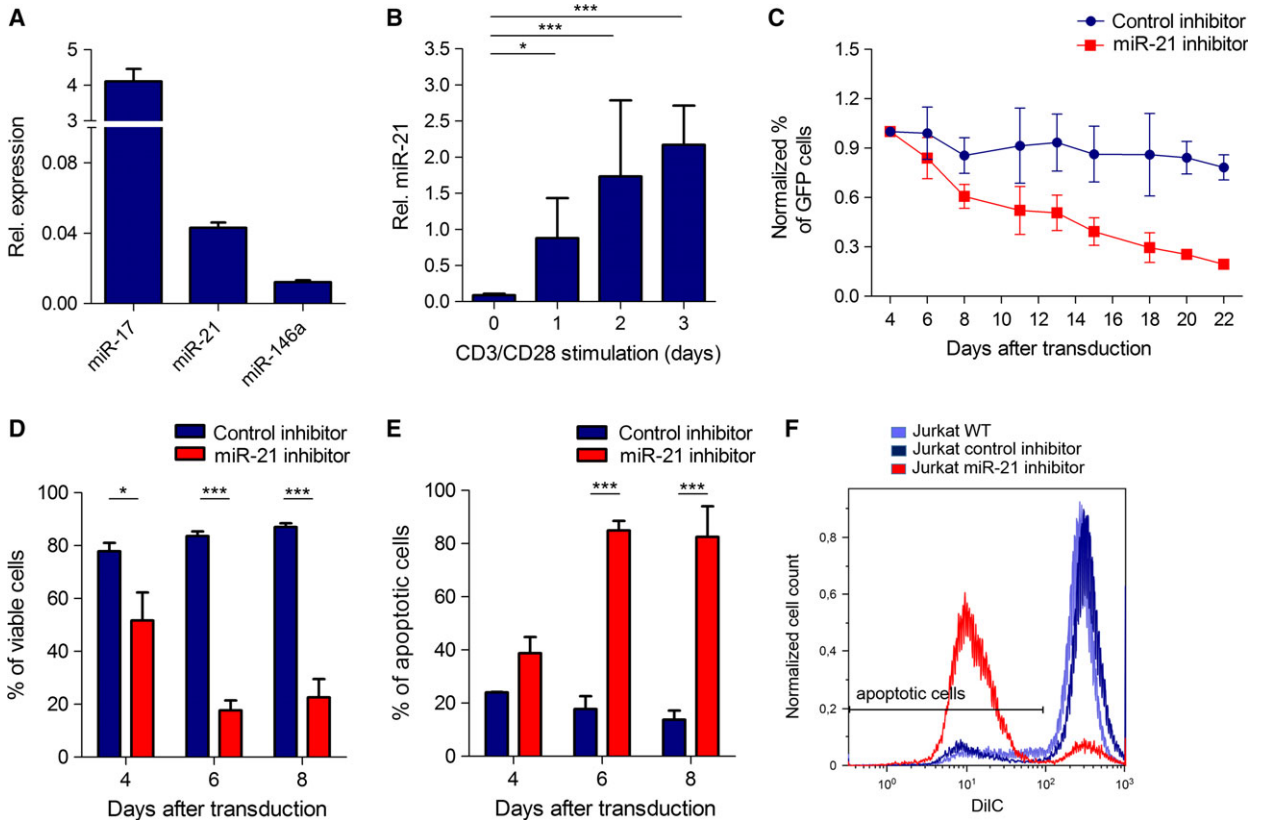

Fig. 1. Validation of the Jurkat cell line as a model to study miR-21 function in T cells. (A) Relative expression of miR-21 in comparison to a randomly picked miRNA with higher (miR-17) and lower (miR-146a) expression as analyzed by qRT-PCR in Jurkat cells. miRNA expression was normalized to the expression of RNU48 (shown is the mean ± error). (B) miR-21 expression levels in Jurkat cells analyzed by qRT-PCR with and without αCD3/αCD28 activation. miR-21 expression was normalized to RNU48 ($n = 4$, Friedman test). Shown is the median with interquartile range. (C) Relative growth of Jurkat cells as determined by a GFP competition assay. Cells were stably transduced with miR-21 inhibitor and control inhibitor vectors that coexpress GFP. The percentage of GFP+ cells in a mixture of transduced and nontransduced cells was followed up for 22 days in three independent experiments. The GFP percentage at day 4 of each sample was set to 1. Mean values with SD are shown ($n = 3$, mixed model analysis). (D) Percentages of viable Jurkat cells upon transduction with control or miR-21 inhibitor based on the forward and side scatter pattern obtained by FACS. Mean values with standard error of mean (SEM) are depicted for control ($n = 3$) and miR-21 inhibitor ($n = 4$, two-way repeated measures ANOVA with a Bonferroni post-test). (E) Percentages of apoptotic Jurkat cells in culture upon transduction with control ($n = 2$) or miR-21 inhibitor ($n = 2$). Apoptotic cells were defined by the loss of mitochondrial transmembrane potential as assessed by FACS analysis using DiLC compound (50 nM). Mean values with SEM are depicted (two-way repeated measures ANOVA with a Bonferroni post-test). (F) Representative FACS plot depicting the increase of apoptotic cells upon miR-21 inhibition as loss of DiLC staining (day 6). $*P \leq 0.05$, $***P \leq 0.001$.

Genes involved in sensitivity to TRAIL-induced apoptosis were found among the top-10 most enriched in Jurkat-miR-21 but not in Jurkat-EV cells (position 1237). The expression levels of genes represented by the latter gene set showed an overall decrease in the total fraction of Jurkat-miR-21 as compared to Jurkat-EV (not shown). These differences can be explained by either direct or indirect effects of miR-21 and fit with the observed antiapoptotic role of miR-21 in Jurkat cells. Comparison of the expression levels of all predicted miR-21 target genes (209 of 14 514 unique genes) between the total fractions of Jurkat-EV and Jurkat-miR-21 revealed a systematic decrease in transcript levels in Jurkat-miR-21 cells (Fig. 3A). This indicates that transcript levels of predicted miR-21 genes were decreased upon miR-21 overexpression. As a control, we also analyzed differences in the expression levels of predicted miR-146a targets (162 of 14 514) and predicted miR-17 targets (929 of 14 514). No difference was observed for the predicted miR-146a target genes, while a mild decrease was observed for predicted miR-17 target genes (Fig. 3A). The latter observation can be explained by the marked overlap between the miR-21 and miR-17 predicted target genes, i.e., 62 shared predicted target genes. In line with these observations, we noted a specific enrichment

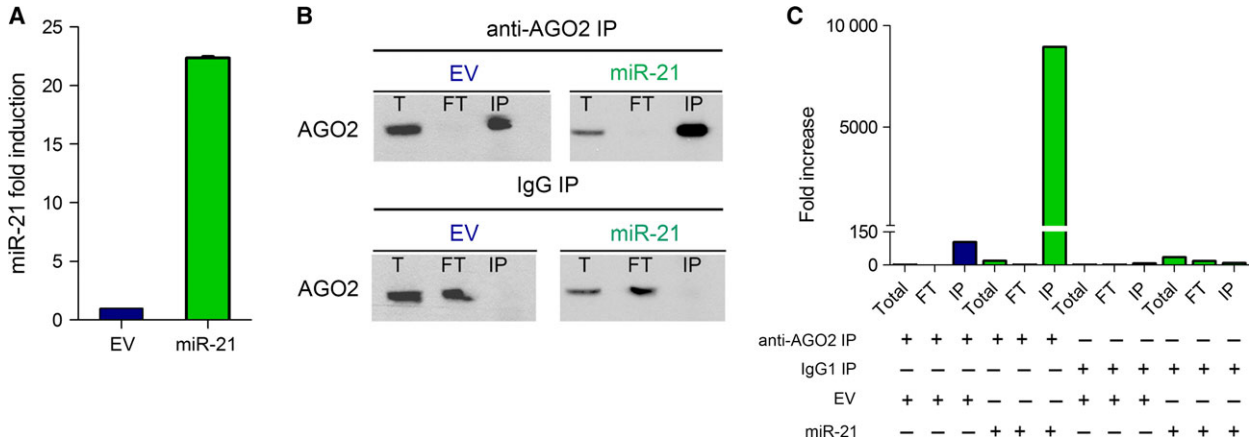

Fig. 2. Efficiency of AGO2-RISC IP in Jurkat-EV and Jurkat-miR-21 cells. (A) qRT-PCR analysis of miR-21 in Jurkat cells transduced with empty vector (EV) or miR-21. miR-21 expression was normalized to RNU48 and the level detected in Jurkat-EV was set to 1 ($n = 3$, median with interquartile range is shown). (B) Western blot analyses for AGO2 to determine the efficiency of the AGO2-IP using total (T), Flowthrough (FT) and immunoprecipitated (IP) fractions of Jurkat-EV and Jurkat-miR-21. IP with mouse IgG1 served as a negative control. (C) qRT-PCR analysis of miR-21 levels in RNA isolated from T, FT, and IP fractions of AGO2- and control IgG1-IP experiments of Jurkat-EV and Jurkat-miR-21 cells. miR-21 expression was normalized to RNU48 and the level detected in the T of Jurkat-EV was set to 1. miR-21 was enriched in the AGO2-IP fractions of Jurkat-EV and Jurkat-miR-21, and was 86-fold higher in the IP fraction of Jurkat-miR-21 as compared to the IP fraction of Jurkat-EV.

Table 1. Gene set enrichment analysis.

	Position in GSEA	
Gene set	EV	miR-21
AGCACTT, miR-93, miR-302A, miR-302B, miR-302C, miR-302D, miR-372, miR-373, miR-520E, miR-520A, miR-526B, miR-520B, miR-520C, miR-520D	2	1
TGAATGT, miR-181A, miR-181B, miR-181C, miR-181D	9	2
GCACTTT, miR-17-5P, miR-20A, miR-106A, miR-106B, miR-20B, miR-519D	1	3
TTTGCAC, miR-19A, miR-19B	8	4
ACACTAC, miR-142-3P	4	5
GTGCAAT, miR-25, miR-32, miR-92, miR-363, miR-367	6	6
TGCACTT, miR-519C, miR-519B, miR-519A	7	7
TTGCACT, miR-130A, miR-301, miR-130B	10	8
HAMAI_APOPTOSIS_VIA_TRAIL_UP	1237	9
SENGUPTA_NASOPHARYNGEAL_CARCINOMA_WITH_LMP1_UP	106	10
ACTTTAT, miR-142-5P	5	17
ATAAGCT, miR-21	46	28
BROCKE_APOPTOSIS_REVERSED_BY_IL6	3	258

of predicted miR-21 target genes among the top-1500 genes enriched in the IP of Jurkat-miR-21 ($n = 72$) as compared to the IP of Jurkat-EV cells ($n = 48$). The enrichment was even more pronounced among the top-250 enriched genes ($n = 20$ versus $n = 10$; Fig 3B). As a control, we also analyzed enrichment of the predicted target genes of miR-146a and miR-17, which revealed no differences between Jurkat-EV and Jurkat-miR-21 (Fig. 3B). Together, these data show an efficient enrichment of miRNA target genes in the IP fractions of both conditions and a marked enrichment of miR-21 predicted target genes in Jurkat cells over-expressing miR-21.

LATS1 is involved in the antiapoptotic role of miR-21 in T cells

Seventy-two predicted miR-21 targets were enriched at least twofold in Jurkat-miR-21 IP as compared to the total fraction. Seventy-one of these 72 targets were

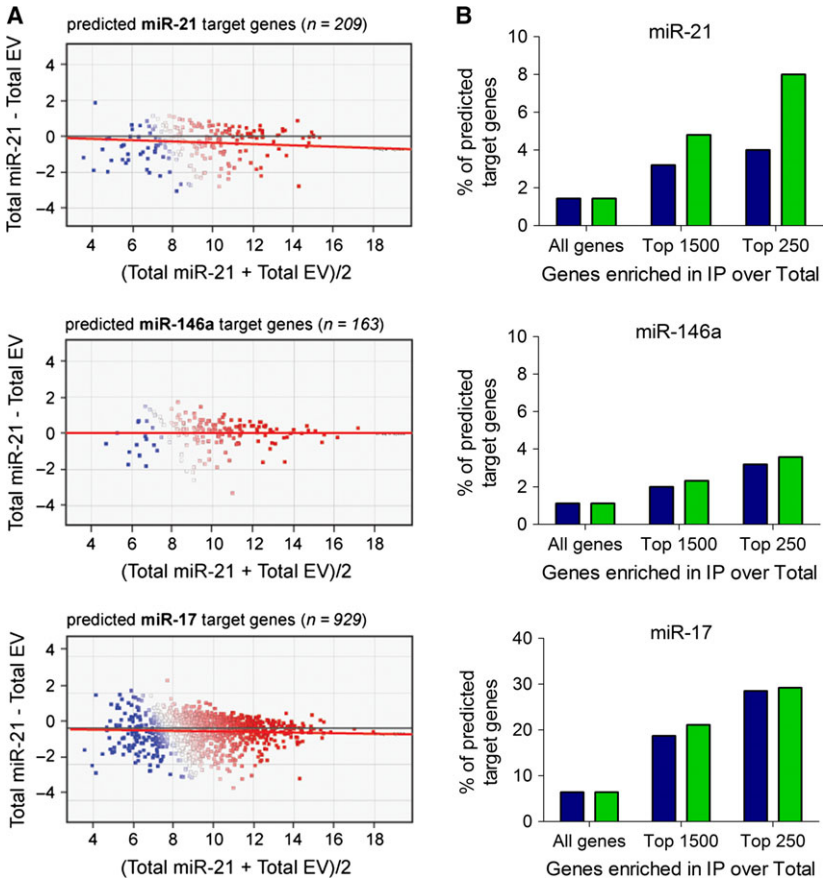

Fig. 3. Transcript levels of predicted miR-21 targets are more enriched in the AGO2-IP fraction and depleted in total fraction upon miR-21 overexpression. (A) Bland–Altman plots comparing the expression levels of miR-21, miR-146a, and miR-17 predicted target genes in the total fractions of Jurkat-EV and Jurkat-miR-21. The expression difference of each gene is plotted against its mean expression. Red lines represent the best fit to the data. (B) Percentages of predicted miR-21, miR-146a, and miR-17 target genes in all 14 514 expressed genes and in the top-1500 and top-250 most enriched genes in the AGO2-IP fractions of Jurkat-EV and Jurkat-miR-21. Filled bars represent miR-21 IP, open bars represent EV IP.

enriched at least twofold more in the AGO2-IP fraction of Jurkat-miR-21 as compared to the AGO2-IP fraction of Jurkat-EV. These 71 targets and their gene ontologies are listed in Table 2 and include 11 previously confirmed miR-21 target genes (at least by reporter assay). Of these 11, we validated the regulation of PIK3R1 by miR-21 using luciferase assays and the upregulation of PDCD4 protein expression upon miR-21 inhibition in Jurkat cells (data not shown). Within the 71 target genes identified in this study, six were related to regulation of apoptosis, i.e., *PDCD4*, *Ras* homology family member B (*RHOB*), mitogen-activated protein kinase 1 (*MAP3K1*), protein kinase C (*PRKCE*), *RAS P21* protein activator (GTPase-activating protein) 1 (*RASA1*), and *LATS1*.

We selected *LATS1* for further studies as it showed the strongest increase in AGO2-IP enrichment upon miR-21 overexpression (Table 2) and had a known function related to apoptosis [17,18]. In addition, it was recently shown that miR-21 can target *LATS1* in cervical cancer [19]. We identified one 8-mer and two 7-mer miR-21-binding sites in the 3′UTR of *LATS1* (Fig. 4A). Luciferase reporter assays with two constructs including either the 8-mer or the two 7-mer miR-21-binding sites consistently showed significant increases in luciferase activity, thereby demonstrating that LATS1 is a bona fide miR-21 target (Fig. 4B). In agreement with this finding, inhibition of miR-21 in Jurkat cells increased the expression of LATS1 protein (Fig. 4C).

To determine the relevance of the increase of LATS1 for the miR-21 inhibition-induced phenotype (Fig. 1C), we studied the effect of miR-21 inhibition in LATS1-knockdown (KD) cells. Stable LATS1-KD cells were generated by infection of Jurkat cells with lentiviral *LATS1*-shRNA constructs or NT control shRNA vectors. Western blotting for LATS1 in sorted LATS1-KD cells showed that the efficiency of the shRNAs ranged between 70% and 90% (Fig. 5A). Next, we infected the LATS1-KD and control cells with miR-21 inhibitor and control inhibitor virus, containing GFP and monitored the GFP percentage over time within the LATS1-KD cells. As expected, miR-21 inhibition caused a strong reduction in the percentage of GFP+ cells in the NT shRNA-infected and wild-type cells with on average 15% of GFP+ cells left after

Table 2. Functional annotation of 71 predicted miR-21 target genes with ≥2-fold increase in IP enrichment upon miR-21 overexpression.

Gene symbol	EV IP/T	miR-21 IP/T	miR-21/EV	Proven target	Annotation
LATS1	4.8	126.9	26.6	[19]	Apoptosis induction, cell cycle inhibition, serine/threonine kinase activity
FAM63B	1.2	19.3	16.5		Phosphoprotein
MBNL1	2.2	34.7	15.8		RNA splicing regulation
TRPM7	1.9	21.8	11.3		Transmembrane protein, cation channel activity
CDK6	0.8	7.8	9.7	[1]	Cell cycle regulation, cyclin-dependent protein kinase activity, p53 signaling pathway
RAB22A	0.8	6.4	7.9		Intracellular signaling cascade, GTPase activity
PAG1	0.9	7	7.8		Immune system, inhibition of lymphocyte activation, molecular adaptor activity
TET1	1.7	13.4	7.8		Oxidoreductase activity
BMPR2	2.5	19.8	7.8	[27]	Phosphorylation induction, serine/threonine kinase activity
PLAG1	7.8	61.2	7.8		Transcription regulation, transcription factor activity
STAG2	0.9	6.5	7.4		Cell cycle regulation, chromosome segregation, mitosis, meiosis
FAM126B	2.4	17.2	7.2		Phosphoprotein
UBN2	1.7	11.8	7		Phosphoprotein
PIK3R1	1.3	9.3	6.9	[28]	Immune system development, lymphocyte activation, TCR signaling
YOD1	2.8	19.6	6.9		Proteolysis, peptidase activity
RPS6KA3	0.6	4.1	6.5		Serine/threonine kinase activity, MAPK signaling pathway
NFAT5	2	12.7	6.4		Immune system, transcription induction, transcription factor activity, TCR signaling
FBXO28	3	18.1	6.1		Proteolysis
LCORL	1.3	7.7	6.1		Transcription regulation
PDCD4	0.9	5.3	5.7	[1,29,30]	Apoptosis induction, cell cycle inhibition, inhibition of kinase activity
PAN3	4.1	23.5	5.7		mRNA catabolism process, protein kinase activity
MSL1	0.9	5.3	5.6		Chromatin organization
PLEKHA1	6	31.3	5.3		Enzyme-linked receptor protein signaling pathway
AP4E1	1	5.1	5.3		Intracellular protein transport
KLHL15	3.4	17.8	5.3		Na
PBRM1	0.7	3.7	5.2		Cell cycle regulation, chromatin regulator
ZYG11B	0.8	4.1	5.1		Proteolysis
CPEB3	4.2	20.9	5		RNA binding
PRPF4B	1	4.8	5		RNA processing, serine/threonine kinase activity
PIKFYVE	0.8	3.9	4.9		Intracellular signaling cascade, phosphatidylinositol signaling system
SATB1	1.5	7.3	4.8		Transcription inhibition, chromatin organization
RASGRP1	1	4.6	4.7	[31]	Immune system, intracellular signaling cascade, TCR signaling
FBXO11	1.2	5.6	4.6	[32]	Proteolysis, ubiquitin ligase complex
PURB	1.5	6.9	4.6		Transcription inhibition, transcription factor activity
WWP1	2	9	4.4		Proteolysis, ubiquitin ligase complex
TOPORS	0.9	3.8	4.4	[33]	Proteolysis, response to DNA damage stimulus
FAM3C	4.7	20.3	4.3		Cytokine activity
BCL11A	2.8	12.2	4.3		Immune system development, lymphocyte activation, transcription repressor activity
C10orf12	0.8	3.5	4.3		Phosphoprotein
KLF12	1	4.1	4.3		Transcription regulation, transcription factor activity
CHIC1	3.2	13.5	4.2		Cytoplasmic membrane-bounded vesicle
SLC10A7	2.5	10.2	4.1		Ion transport, organic acid: sodium symporter activity
RASA1	1.6	6.2	3.9	[31,34]	Apoptosis inhibition, GTPase activity, MAPK signaling pathway
SECISBP2L	1.7	6.4	3.9		Phosphoprotein
FRS2	5.4	20.6	3.8		Cell–cell signaling, phosphorylation regulation, phosphatase regulator activity
TRIM33	1	3.9	3.7		Transcription inhibition
EIF2C4	1.1	4.2	3.7		Translation inhibition, ribonucleoprotein complex
ZNF217	3.3	12	3.6		Transcription regulation, transcription factor activity
CHD7	1	3.6	3.5		Immune system development, lymphocyte activation, helicase activity
NFIA	1.1	3.9	3.4		Transcription regulation, transcription factor activity

Table 2. (Continued).

Gene symbol	EV IP/T	miR-21 IP/T	miR-21/EV	Proven target	Annotation
SKI	2.5	8.1	3.3		Transcription inhibition, transcription factor activity
C5orf41	7.5	24.5	3.3		Transcription regulation, transcription factor activity
ZNF367	13.7	38.5	2.8		Transcription regulation, transcription factor activity
EIF4EBP2	3.3	9.3	2.8		Translation inhibition
RECK	2.7	7.5	2.8	[35]	Vasculature development, peptidase inhibitor activity
MARCH5	2.9	7.5	2.6		Proteolysis
TNRC6B	1.4	3.6	2.6		Translation inhibition, ribonucleoprotein complex
RHOB	1.9	4.8	2.5	[36]	Apoptosis induction, cell cycle inhibition, GTPase activity
AP3M1	1.4	3.6	2.5		Intracellular protein transport
ATPAF1	2.1	5.2	2.5		Protein complex assembly, mitochondrion
KBTBD6	1.9	4.7	2.5		Proteolysis
PPP1R3B	2	4.8	2.4		Insulin signaling pathway, glucose metabolism process
ZFP36L2	2.5	6	2.4		mRNA stability regulation, transcription factor activity
BCL7A	2.7	6.5	2.4		Transcription inhibition
MAP3K1	1.5	3.4	2.3		Apoptosis induction, stress-activated protein kinase signaling, MAPK signaling
C17orf39	2.7	6.3	2.3		Na
CNOT6	1.8	4.2	2.3		Transcription regulation, nuclease activity
CD69	31.9	72.6	2.3		Transmembrane protein
KLF3	2.1	4.4	2.1		Transcription regulation, transcription factor activity
PRKCE	2.1	4.1	2		Apoptosis inhibition, calcium-independent protein kinase C activity
SLC7A6	1.8	3.7	2		Organic acid transport, amino acid transmembrane transporter activity

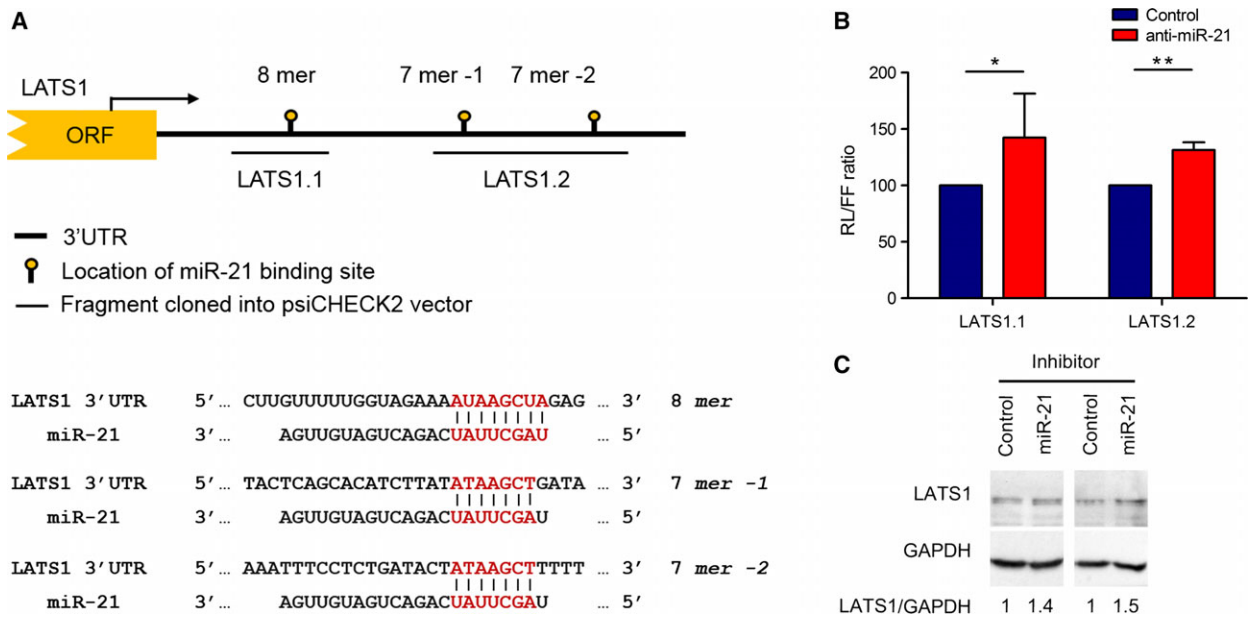

Fig. 4. Luciferase reporter assay for LATS1 3′UTR. (A) Schematic presentation of the location of the miR-21-binding sites in the 3′UTR of LATS1 and the regions cloned into the reporter vector. Binding site sequences are shown in the lower part. (B) Luciferase reporter assay shows that miR-21 can bind to the miR-21-binding sites in LATS1. Plotted is the ratio of Renilla luciferase (RL) to firefly luciferase (FL) signal detected in lysates of Cos-7 cells transfected with psiCHECK-2 construct and cotransfected with miR-21 inhibitor (closed bars) or control inhibitor (open bars). Shown per condition is the mean with SD ($n = 5$, unpaired t-test) (C) Quantification of LATS1 protein levels in Jurkat cells transduced with control or miR-21 inhibitor. Results from two independent experiments are shown, analyzed by western blot. A representative image of each experiment is shown. GAPDH was used as internal control. LATS1 to GAPDH ratio in control inhibitor-infected cells was set to 1. $*P \leq 0.05$, $**P \leq 0.01$.

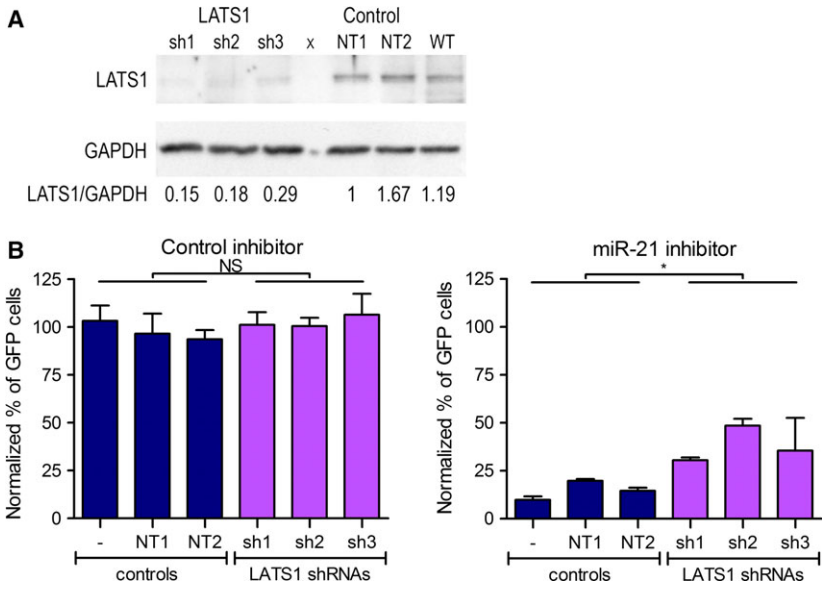

Fig. 5. LATS1 knockdown can partially rescue the miR-21 inhibition-induced impaired cell growth phenotype. (A) Analysis of LATS1 protein levels upon knockdown in Jurkat cells. Jurkat cells were stably infected with shRNA constructs targeting LATS1 or NT control shRNAs and sorted based on dsRED fluorescence. WT = wild-type. LATS1 levels relative to GAPDH are shown below. (B) LATS1 knockdown cells are less susceptible to miR-21 inhibition-induced impaired growth. Sorted LATS1 KD cells (sh1-sh3, black bars) and controls (NT1, NT2, and WT, white bars) were infected with miR-21 inhibitor or control inhibitor cells. miR-21 or control inhibitor-infected cells were followed based on GFP fluorescence, and the GFP percentage within the LATS1 knockdown cells was monitored till day 22 post infection. For each sample, the GFP percentage at day 4 was set to 100% and the relative percentage at day 22 post infection is indicated. The GFP percentage remains unaffected in control inhibitor-infected cells. In contrast, most GFP+ cells are gone in miR-21 inhibitor-infected cells. LATS1 knockdown cells have on average more than 2.5-fold more GFP+ cells left than the controls indicating that LATS1 knockdown can partially rescue the miR-21 inhibition-induced phenotype. Shown is the mean with SD ($n = 2$, unpaired t-test). *P-value ≤ 0.05.

22 days (Fig. 5B). Knockdown of LATS1 was found to partially rescue this effect as a more than 2.5-fold higher percentage of GFP+ cells was left (average of the three shRNAs, 38%) after 22 days of miR-21 inhibition (P-value ≤ 0.05, Fig. 5B). These results show that the proapoptotic effect observed upon miR-21 inhibition is at least in part mediated by downregulation of LATS1.

To study the relevance of the miR-21–LATS1 axis in primary T cells, we analyzed *LATS1* and miR-21 levels of primary sorted naïve T cells (CD4+CD45RO-) stimulated for 3 days with α-CD3 and α-CD28. This revealed an inverse pattern, i.e., increased levels of miR-21 and decreased levels of *LATS1* upon stimulation (Fig. 6A, B). The increase of miR-21 upon stimulation supports our previous findings and those of others [11–13,20]. The inverse expression pattern of *LATS1* suggests that targeting of LATS1 by miR-21 is highly relevant for survival of primary T cells. We also studied miR-21 and LATS1 expression in sorted naïve (CD4+CD45RO-) and memory (CD4+CD45RO+) T cells. In line with what we and others have previously shown, we observed higher levels of miR-21 in memory T cells compared to naïve T cells (Fig. 6C) [11,12,20]. However, we did not observe decreased LATS1 transcript levels in memory T cells as compared to naïve T cells (Fig. 6D). This suggests that miR-21 does not lower the LATS1 RNA levels in memory cells, but regulates LATS1 protein level by post-transcriptional repression of protein translation. To confirm regulation of LATS1 protein levels by miR-21 specifically in memory T cells, LATS1 protein analysis in naïve and memory T cells as well as AGO2-RIP experiments should be performed.

In summary, we showed that the Jurkat cell line is a suitable model to study the role of miR-21 in the regulation of T-cell apoptosis. We experimentally identified multiple miR-21 target genes via employing AGO2-RIP-Chip, including the proapoptotic LATS1 gene. We showed that LATS1 is a bona fide miR-21 target whose knockdown can at least partially rescue the proapoptotic effect of miR-21 inhibition. Thus, LATS1 is likely to be an important target for the antiapoptotic role of miR-21 in (activated) T cells, possibly in combination with other targets such as PDCD4. As miR-21 is widely overexpressed in a variety of cancers, it is also of interest to further study the relevance of the miR-21 target LATS1 in relation to cancer.

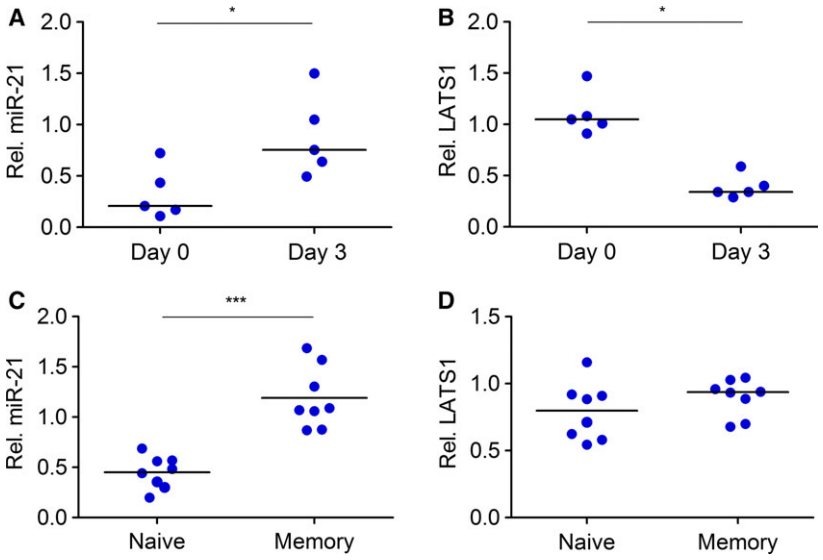

Fig. 6. Expression of miR-21 and LATS1 in primary CD4+ T cells. Analysis of (A) miR-21 and (B) LATS1 mRNA expression in CD3+CD4+CD45RO- naive T cells before and after 3 days of stimulation with αCD3/CD28. Analysis of (C) miR-21 and (D) LATS1 expression in sorted CD3+CD4+CD45RO- naïve and CD3+CD4+CD45RO+ memory T cells. miR-21 expression was normalized to RNU44, and LATS1 levels were normalized to TBP. Data are presented as relative expression and medians are indicated as a horizontal line (panel A and B: $n = 5$, panel C and D: $n = 8$, Mann–Whitney test). $^{*}P \leq 0.05$, $^{***}P \leq 0.001$.

Materials and methods

Cell lines

The Jurkat, human acute leukemic T-cell line was cultured in RPMI 1640 supplemented with 10% fetal bovine serum (FBS), 200 mM L-glutamine, 100 mM Na-pyruvate, 10 mg·mL^{-1} gentamycin (Lonza, Breda, The Netherlands), 0.05 M β-mercapto-ethanol (Merck, Darmstadt, Germany) at 37 °C in 5% CO_2. The SV40 large T-antigen-transformed human embryonic kidney cell line, HEK293T, and Phoenix-Ampho were cultured in Dulbecco's modified Eagle's medium (DMEM) supplemented with 10% FBS, 200 mM L-glutamine, and 10 mg·mL^{-1} gentamycin sulfate (Lonza) at 37 °C in 5% CO_2. African Green Monkey SV40-transformed kidney fibroblast cell line COS-7 was cultured in DMEM supplemented with 10% FBS (Thermo Scientific, Breda, The Netherlands), 200 mM L-glutamine, and 10 mg·mL^{-1} gentamycin sulfate at 37 °C in 5% CO_2. Cell lines were obtained from ATCC. We routinely confirmed the identity of our cell lines using the PowerPlex 16 HS System (Promega, Leiden, The Netherlands).

T-cell activation with αCD3/αCD28 monoclonal antibodies (mAbs)

Stimulation of Jurkat T cells was performed with plate-bound anti-CD3 and soluble anti-CD28 mAbs. Briefly, culture plates were incubated with goat anti-mouse-IgG2a Ab (Cat. No. 1080-01, Southern Biotechnology, Uden, The Netherlands) overnight at 4 °C, followed by washing with PBS and 1-h incubation with hybridoma-culture supernatant, containing anti-human-CD3 IgG2a mAb (clone WT32, concentration ~ 1 μg IgG·mL^{-1}) at RT. Unbound anti-CD3 antibody was removed by washing 4 times with an excess of PBS. Cells were seeded at a density of 0.25×10^6 cells·mL^{-1} in medium supplemented with 5% V/V hybridoma-culture supernatant containing anti-CD28 IgG1 mAb (clone 20-4669), resulting in a final concentration of 0.1 μg IgG·mL^{-1}. At the indicated time points, cells were harvested, lyzed with Qiazol reagent (Qiagen, Venlo, The Netherlands), and stored at −20 °C. Primary CD4+ T-cell isolation and stimulation was described earlier [20,21]. All participants provided written informed consent according to the Declaration of Helsinki to participate in this study which was approved by The Medical Ethical Committee (METC; project number: 2009.118) of the University Medical Center Groningen UMCG.

Viral constructs

To generate the lentiviral miR-21 overexpression construct, pre-miR-21 with ~ 150 nucleotides of the flanking sequence was amplified from genomic DNA using forward 5′-gtcagaatagaatagaattgggg-3′ and reverse 5′-gctgcattatggcacaaaag-3′ primers. *Nhe*I and *Xho*I restriction sites were added to the forward primer and an *Eco*RI site was added to the reverse primer to allow directional cloning into the retroviral MXW-PGK-IRES-GFP vector [22] using standard laboratory procedures. To stably inhibit miR-21 function, we used a lentiviral miR-21 inhibition vector (pmiRZip-21; Cat. Nr: MZIP21-PA-1) and three NT lentiviral inhibitor vectors (control inhibitor, Cat. Nr: MZIP000-PA-1, both from Systems Biosciences, Mountain View, USA and shNT1 and shNT2, see below) as controls. The sequences of shRNAs against *LATS1* and controls used for cloning to the *Bam*HI and *Eco*RI sites of the lentiviral pDsREDPuro vector (MZIP/pGreenPuro vector with the copGFP replaced by dsRED, Systems Biosciences) are as follows: *LATS1-sh1-S:* 5′GATCCGCTGCTCCT TCGTCATATACATTCAAGAGATGTATATGACGAAGG

AGCAGCTTTTTG3′, *LATS1-sh1-AS:* 5′AATTCAAAA AGCTGCTCCTTCGTCATATACATCTCTTGAATGTA TATGACGAAGGAGCAGCG3′, *LATS1-sh2-S:* 5′GATC CGAAATCAAGTCGCTCATGTTATTCAAGAGATAAC ATGAGCGACTTGATTTCTTTTTG3′, *LATS1-sh2-AS:* 5′AATTCAAAAAGAAATCAAGTCGCTCATGTTATCT CTTGAATAACATGAGCGACTTGATTTCG3′, *LATS1-sh3-S:* 5′GATCCGTCTGCTTCATACATTCCTAATTCA AGAGATTAGGAATGTATGAAGCAGACTTTTTG3′, *LA TS1-sh3-AS:* 5′AATTCAAAAAGTCTGCTTCATACATT CCTAATCTCTTGAATTAGGAATGTATGAAGCAGAC G3′, *shNT1-S:* 5′GATCCGCTAAGGTTAAGTCGCCC TCGCTTTCAAGAGAAGCGAGGGCGACTTAACCTT AGGTTTTTG3′, *shNT1-AS:* 5′AATTCAAAAACCTAAG GTTAAGTCGCCCTCGCTTCTCTTGAAAGCGAGGG-CGACTTAACCTTAGCG3′, *shNT2-S:* 5′GATCCGCAAC AAGATGAAGAGCACCAACTCTTCAAGAGAGTTGT-TCTACTTCTCGTGGTTGAGTTTTTG3′, *shNT2-AS:* 5′A ATTCAAAAACTCAACCACGAGAAGTAGAACAACT-CTCTTGAAGAGTTGGTGCTCTTCATCTTGTTGCG3′.

Virus production and viral transduction

Lentiviral particles were produced with a third-generation lentiviral system in 293T cells by $CaPO_4$ transfection as described previously [23]. Lentiviral transduction of Jurkat cells was carried out for 24 h in the presence of 4 $\mu g \cdot mL^{-1}$ polybrene (Sigma-Aldrich, St. Louis, USA).

Retroviral particles were produced by calcium phosphate ($CaPO_4$)-mediated transfection of Phoenix-Ampho packaging cells with 10 μg pMXW-PGK-IRES-GFP-miR-21 (miR-21 overexpression) or pMXW-PGK-IRES-GFP-EV (control) and 0.63 μg of pSuper-DGCR8 in T25 flask. Retroviral particles were collected 48 h after transfection, passed through a 0.45 μm Millex-HV filter (Millipore, Amsterdam, The Netherlands) and concentrated with Retro-X concentrator (Clontech, Saint-Germain-en-Laye, France) according to the manufacturer's protocol. Jurkat cells were transduced with the virus by spinning at 1200 ***g*** for 2 h.

GFP competition assay

GFP percentage of pmiRZip-21- or pmiRZip-scrambled-infected Jurkat cells was followed over a period of 22 days. The starting GFP percentage varied between 30% and 40%. Data were acquired on FACS Calibur flow cytometer (BD Biosciences, San Jose, CA, USA) and analyzed using FLOWJO software (version 7.6, Treestar, Ashland, OR, USA). The GFP percentage analyzed at the first day of measurement (day 4) was set to 1. The GFP competition assay was performed 3 times.

Apoptosis measurement

Percentages of apoptotic cells were assessed in Jurkat cells transduced with miR-21 or control inhibitor in > 95% of the cells on day 4, 6, and 8 following viral transduction by FACS-based measurement of mitochondrial transmembrane potential loss. Briefly, cells were stained for 20 min at 37 °C in cell culture medium containing 50 nM DiLC1 (Enzo Life Sciences, NY, USA), which was followed by a washing step with PBS. Cells were kept on ice and DiLC1 staining was measured at the FACS Calibur flow cytometer using Cell Quest software (BD Biosciences). Data were analyzed using Kaluza Flow Analysis Software (Beckman Coulter).

Quantitative RT-PCR

Total cellular RNA was extracted using the miRNeasy Mini Kit (Qiagen) following the manufacturer's instructions. The RNA quantity was measured on a NanoDrop ND-1000 Spectrophotometer (Thermo Scientific).

MicroRNA expression levels were determined by quantitative RT-PCR. RNA was reverse transcribed using the Taqman miRNA Reverse Transcription kit in combination with multiplexed reverse transcription primers of TaqMan miRNA assays (Thermo Scientific): for miR-21-5p (ID: 000397), miR-17 (ID: 002308), miR-146a (ID: 000468), RNU48 (ID: 001006), RNU44 (ID: 001094) [24]. RNU44 and 48 served as reference genes to normalize miRNA expression levels. The qPCR reaction was performed using qPCR MasterMix Plus (Eurogentec, Liege, Belgium).

cDNA synthesis for mRNA was performed using Superscript III RTase (Thermo Scientific). The qPCR reaction was performed using qPCR MasterMix Plus. Taqman gene assay was used for detection of *LATS1*: Hs01125523_m1; Thermo Scientific). Primers and probe (Integrated DNA Technologies, Coralville, USA) used for detection of TBP were as follows: forward 5′-GCCCGAAACGCCGAAT AT-3′, reverse 5′-CCGTGGTTCGTGGCTCTCT-3′. Mean cycle threshold (C_t) values were quantified with the Sequence Detection Software (SDS, version 2.3, Thermo Scientific), using ABI7900HT thermo cycler (Thermo Scientific). Relative expression levels were determined using the $2^{-\Delta Ct}$ formula, where $\Delta Ct = Ct_{gene} - Ct_{ref.gene}$.

AGO2-RIP-Chip procedure

Immunoprecipitation of AGO2-containing RISC complexes was performed as described previously by Tan *et al.* [15] and Slezak-Prochazka *et al.* [25]. Briefly, cleared lysates of 40 million cells were incubated with protein G Sepharose beads (GE Healthcare, Eindhoven, The Netherlands) coated with anti-AGO2 antibody (Clone 2E12-1C9, Abnova, Taiwan) at 4 °C overnight. IP with anti-IgG antibody was used as a negative control (Millipore BV, Amsterdam, The Netherlands). After washing the beads, RNA was harvested for microarray and qRT-PCR analysis and protein lysates were prepared for western blot. RNA from total (sample taken before start of the IP procedure), flow

through (FT; sample taken of the supernatant after collection of the IP fraction), and IP fractions was isolated with miRNeasy Mini kit (Qiagen) according to the manufacturer's protocol. RNA from total and AGO2-IP fractions of Jurkat-miR-21 and Jurkat-EV cells was used for microarray analysis. Labeling and hybridization were performed using two-color Low Input Quick Amp Labeling Kit, according to the manufacturer's protocol (Agilent, Santa Clara, USA). Briefly, 40–100 ng of RNA from T and AGO2-IP samples was used for cDNA synthesis, followed by cRNA amplification and Cy-3 and Cy-5 labeling. cRNA was purified with RNeasy Kit (Qiagen) and quantified on NanoDrop™ ND-1000 Spectrophotometer (Thermo Scientific). Equal amounts of cRNA Cy-3 and Cy-5-labeled samples were combined and hybridized at 65 °C for 17 h on the 60k SurePrint G3Human Whole Genome Oligo Microarray (Agilent). Next, slides were washed and scanned with SureScan Dx Microarray Scanner (Agilent). Scanned images were used for Agilent Feature Extraction software version 10.5, converted into Linear and Lowess normalized data. Quality control report was generated for each array. Using GeneSpring GX version 12.5 (Agilent), quantile normalization of the signals was performed. Next, probes not detected in more than half of the samples and probes that are inconsistent (more than twofold different) in Cy-3 and Cy-5 replicates of the same sample were filtered out. The averaged signals for Cy-3 and Cy-5 replicates were used to calculate the IP/T ratio for each sample. The microarray data have been deposited in NCBI's Gene Expression Omnibus (GSE85116).

Western blotting

Cells were lyzed in Cell Lysis buffer (Cat. # 9803, Cell Signaling Technologies, Leiden, The Netherlands) and incubated on ice for 45 min, centrifuged at 14 000 ***g***, 4 °C and supernatant was collected. Protein concentration was determined using DC Protein Assay following the manufacturer's instructions (Bio-Rad Laboratories, Hercules, USA). Samples were separated on 10% polyacrylamide gels and transferred onto nitrocellulose membranes. Membranes were blocked using Odyssey blocking buffer (LI-COR Biosciences, Nebraska, USA). For the detection of LATS1, rabbit polyclonal anti-human-LATS1 antibody (ab 70562; Abcam, Cambridge, UK) was used in a dilution of 1 : 250 and incubated overnight at 4 °C. LATS1 expression was visualized with secondary polyclonal antibody goat anti-rabbit peroxidase (GaRPO) 1 : 1000 incubated at RT for an hour (Dako, Leuven, Belgium) and a tertiary rabbit-anti-goat peroxidase (RAGPO) incubation step (1-h incubation, 1 : 1000 at RT; Dako). The GAPDH antibody (Santa Cruz Biotechnology, Santa Cruz, USA) was used in a 1 : 20 000 dilution and staining was visualized with secondary polyclonal rabbit-anti-mouse peroxidase (RaMPO, 1 : 1000). All antibodies were diluted in Odyssey blocking buffer supplemented with 0.1% Tween-20. Immunoblots were incubated with primary antibodies at 4 °C overnight. Secondary polyclonal goat anti-mouse antibody conjugated with IRdye 680, and polyclonal goat anti-rabbit antibody conjugated with IRdye 800 (both from LI-COR Biosciences) were used. Signal was detected with the Odyssey Infrared Imaging System, Odyssey CLx, and protein bands were visualized and quantified with IMAGE STUDIO software version 2.0.38 (both from LI-COR Biosciences). Western blot for AGO2 was performed as described previously [25].

Cloning of 3′-UTRs in reporter constructs, transient transfection, and luciferase assays

3′UTR sequences of *LATS1* (*LATS1.1*/*LATS1.2*) harboring miR-21-binding sites were PCR amplified from genomic DNA using primers with an *Xho*I (forward) or *Not*I (reverse) restriction site, for *LATS1.1* forward: 5′-AAGGAGA AACCTGGTATCTAT-3′, reverse 5′-GAAACTAAGGAA TACAGGG-3′ and LATS1.2 forward: 5′-AAATTGCTGA TACCAAAGG-3′, reverse 5′-GGAGGGGACTGAAATG TTAGG-3′ and cloned into psiCHECK2 vector (Promega, Madison, USA), as previously described [26]. The inserts were sequence verified (BaseClear, Leiden, The Netherlands). About 1.2×10^4 Cos-7 cells were transfected with 125 ng of the psiCHECK2 construct and 50 nM miR-21 inhibitor, molecule ID: 4102261-101 or Negative Control #1 inhibitor, (Exiqon, Vedbaek, Denmark), using the Saint-MIX compound (Synvolux Therapeutics B.V., Groningen, The Netherlands), in 250 µl serum-free medium. Four hours following the transfection, 500 µl of medium supplemented with 10% FBS was added. Cells were lysed 24 h after transfection, and Renilla and firefly luciferase activity was measured using the Dual-Luciferase Reporter Assay System (Promega, Leiden, The Netherlands) according to the manufacturer's instructions. For each transfection, luciferase activity was measured in duplicate with the Luminoscan Ascent Microplate Luminometer (Thermo Scientific). The renilla (RL) over firefly (FF) luciferase ratio for miR-21 inhibitor was calculated. The RL/FF ratio of negative control was set to a value of 1. Transfections were performed in triplicate.

Prediction of miRNA target genes

The miRNA target prediction program TARGETSCAN 6.2 (http://www.targetscan.org/) was used to determine predicted target genes of miR-21 (307 conserved genes), miR-146a (224 conserved genes), and miR-17 (1.220 conserved genes).

Functional annotation analysis

The functional annotation of genes was performed using the DAVID BIOINFORMATIC RESOURCES 6.7 (https://david.ncifcrf.

gov/), based on the following GO categories: GOTERM_BP_FAT, GOTERM_CC_FAT, GOTERM_MF_FAT, KEGG_PATHWAY, and SP_PIR_KEYWORDS. About 1–4 GO terms were considered for description of each gene.

Gene set enrichment analysis

Gene sets significantly enriched in the AGO2-IP in comparison to T fraction of Jurkat-EV and Jurkat-miR-21 were determined by the GSEA using the Molecular Signatures Database (GSEA; http://software.broadinstitute.org/gsea/index.jsp) [16]. Lists containing the expression values of 14 415 genes detected in IP and total fractions of Jurkat-EV or Jurkat-miR-21 were uploaded for the analysis.

Statistical analysis

For comparison of qRT-PCR data of nonstimulated and stimulated Jurkat cells, we applied the Friedman repeated measurements nonparametric test. Data from day 0 were compared to other days of stimulation (days 1, 2, 3). For comparison of viable and apoptotic Jurkat cells upon transduction with control or miR-21 inhibitor, we applied two-way repeated measures ANOVA with a Bonferroni post-test. To determine whether miR-21-inhibited cells have a significant impaired cell growth as compared to control inhibitor-infected cells, we performed mixed model analysis as described previously [25]. Significance for (RL/FL) luciferase ratios between control and miR-21 inhibitor was calculated using unpaired *t*-test. The same test was used to determine whether the remaining percentages of GFP+ cells in LATS1-KD group (LATS1 sh1-3) infected with a miR-21 inhibitor were significantly different from the remaining GFP percentages within the controls group (wild-type, NT1 and NT2) infected with a miR-21 inhibitor. For comparisons of *LATS1* and miR-21 in nonstimulated and stimulated CD4+ T cells, we applied the Mann–Whitney test. Statistical analysis were performed with GRAPHPAD Prism version 5.0 (GRAPHPAD Software, San Diego, CA, USA) or SPSS Statistics version 22.0 (IBM Corp. Armonk, NY, USA).

Acknowledgements

We thank healthy young volunteers for participating in the study. We are grateful for the support of the flow cytometry team Roelof Jan van der Lei, Geert Mesander, and Henk Moes.

Author contributions

NT, KSC, BJK, AB, and JK planned experiments. NT, KSC, YY, AS, DJ, BR, PJ, and RJL performed experiments. NT, KSC, YY, ISP, BR, PJ, AMB, BJK, AB, and JK analyzed data. NT, KSC, EB, AMB, BJK, AB, and JK wrote the manuscript.

References

1 Frankel LB, Christoffersen NR, Jacobsen A, Lindow M, Krogh A & Lund AH (2008) Programmed cell death 4 (PDCD4) is an important functional target of the microRNA miR-21 in breast cancer cells. *J Biol Chem* **283**, 1026–1033.
2 Chan JA, Krichevsky AM & Kosik KS (2005) MicroRNA-21 is an antiapoptotic factor in human glioblastoma cells. *Cancer Res* **65**, 6029–6033.
3 Meng F, Henson R, Wehbe-Janek H, Ghoshal K, Jacob ST & Patel T (2007) MicroRNA-21 regulates expression of the PTEN tumor suppressor gene in human hepatocellular cancer. *Gastroenterology* **133**, 647–658.
4 Zhu S, Wu H, Wu F, Nie D, Sheng S & Mo YY (2008) MicroRNA-21 targets tumor suppressor genes in invasion and metastasis. *Cell Res* **18**, 350–359.
5 Zhang JG, Wang JJ, Zhao F, Liu Q, Jiang K & Yang GH (2010) MicroRNA-21 (miR-21) represses tumor suppressor PTEN and promotes growth and invasion in non-small cell lung cancer (NSCLC). *Clin Chim Acta* **411**, 846–852.
6 Rossi S, Shimizu M, Barbarotto E, Nicoloso MS, Dimitri F, Sampath D, Fabbri M, Lerner S, Barron LL, Rassenti LZ *et al.* (2010) MicroRNA fingerprinting of CLL patients with chromosome 17p deletion identify a miR-21 score that stratifies early survival. *Blood* **116**, 945–952.
7 Schramedei K, Morbt N, Pfeifer G, Lauter J, Rosolowski M, Tomm JM, von Bergen M, Horn F & Brocke-Heidrich K (2011) MicroRNA-21 targets tumor suppressor genes ANP32A and SMARCA4. *Oncogene* **30**, 2975–2985.
8 Zhu S, Si ML, Wu H & Mo YY (2007) MicroRNA-21 targets the tumor suppressor gene tropomyosin 1 (TPM1). *J Biol Chem* **282**, 14328–14336.
9 Buscaglia LE & Li Y (2011) Apoptosis and the target genes of microRNA-21. *Chin J Cancer* **30**, 371–380.
10 Meisgen F, Xu N, Wei T, Janson PC, Obad S, Broom O, Nagy N, Kauppinen S, Kemény L, Ståhle M *et al.* (2012) MiR-21 is up-regulated in psoriasis and suppresses T cell apoptosis. *Exp Dermatol* **21**, 312–314.
11 Smigielska-Czepiel K, van den Berg A, Jellema P, Slezak-Prochazka I, Maat H, van den Bos H, van der Lei RJ, Kluiver J, Brouwer E, Boots AM *et al.* (2013) Dual role of miR-21 in CD4+ T-cells: activation-induced miR-21 supports survival of memory T-cells and regulates CCR7 expression in naive T-cells. *PLoS One* **8**, e76217.
12 Carissimi C, Carucci N, Colombo T, Piconese S, Azzalin G, Cipolletta E, Citarella F, Barnaba V, Macino G & Fulci V (2014) MiR-21 is a negative modulator of T-cell activation. *Biochimie* **107**(Pt B), 319–326.

13 Ruan Q, Wang P, Wang T, Qi J, Wei M, Wang S, Fan T, Johnson D, Wan X, Shi W *et al.* (2014) MicroRNA-21 regulates T-cell apoptosis by directly targeting the tumor suppressor gene Tipe2. *Cell Death Dis* **5**, e1095.
14 Smigielska-Czepiel K, van den Berg A, Jellema P, van der Lei RJ, Bijzet J, Kluiver J, Boots AM, Brouwer E & Kroesen BJ (2014) Comprehensive analysis of miRNA expression in T-cell subsets of rheumatoid arthritis patients reveals defined signatures of naive and memory Tregs. *Genes Immun* **15**, 115–125.
15 Tan LP, Seinen E, Duns G, de Jong D, Sibon OC, Poppema S, Kroesen BJ, Kok K & van den Berg A (2009) A high throughput experimental approach to identify miRNA targets in human cells. *Nucleic Acids Res* **37**, e137.
16 Subramanian A, Kuehn H, Gould J, Tamayo P & Mesirov JP (2007) GSEA-P: a desktop application for gene set enrichment analysis. *Bioinformatics* **1**, 3251–3253.
17 Yang X, Li DM, Chen W & Xu T (2001) Human homologue of Drosophila lats, LATS1, negatively regulate growth by inducing G(2)/M arrest or apoptosis. *Oncogene* **20**, 6516–6523.
18 Xia H, Qi H, Li Y, Pei J, Barton J, Blackstad M, Xu T & Tao W (2002) LATS1 tumor suppressor regulates G2/M transition and apoptosis. *Oncogene* **21**, 1233–1241.
19 Liu S, Song L, Zhang L, Zeng S & Gao F (2015) miR-21 modulates resistance of HR-HPV positive cervical cancer cells to radiation through targeting LATS1. *Biochem Biophys Res Commun* **459**, 679–685.
20 Teteloshvili N, Smigielska-Czepiel K, Kroesen BJ, Brouwer E, Kluiver J, Boots AM & van den Berg A (2015) T-cell activation induces dynamic changes in miRNA expression patterns in CD4 and CD8 T-cell subsets. *Microrna* **4**, 117–122.
21 Teteloshvili N, Kluiver J, van der Geest KS, van der Lei RJ, Jellema P, Pawelec G, Brouwer E, Kroesen BJ, Boots AM & van den Berg A (2015) Age-associated differences in miRNA signatures are restricted to CD45RO negative T cells and are associated with changes in the cellular composition, activation and cellular ageing. *PLoS One* **10**, e0137556.
22 Mao TK & Chen CZ (2007) Dissecting microRNA-mediated gene regulation and function in T-cell development. *Methods Enzymol* **427**, 171–189.
23 Winkle M, van den Berg A, Tayari M, Sietzema J, Terpstra M, Kortman G, de Jong D, Visser L, Dierpstra A, Kok A *et al.* (2015) Long noncoding RNAs as a novel component of the Myc transcriptional network. *FASEB J* **29**, 2338–2346.
24 Kluiver J, Slezak-Prochazka I & van den Berg A (2013) Studying microRNAs in lymphoma. *Methods Mol Biol* **971**, 265–276.
25 Slezak-Prochazka I, Kluiver J, de Jong D, Smigielska-Czepiel K, Kortman G, Winkle M, Rutgers B, Koerts J, Visser L, Diepstra A *et al.* (2016) Inhibition of the miR-155 target NIAM phenocopies the growth promoting effect of miR-155 in B-cell lymphoma. *Oncotarget* **7**, 2391–2400.
26 Gibcus JH, Tan LP, Harms G, Schakel RN, de Jong D, Blokzijl T, Möller P, Poppema S, Kroesen BJ & van den Berg A (2009) Hodgkin lymphoma cell lines are characterized by a specific miRNA expression profile. *Neoplasia* **11**, 167–176.
27 Qin W, Zhao B, Shi Y, Yao C, Jin L & Jin Y (2009) BMPRII is a direct target of miR-21. *Acta Biochem Biophys Sin* **41**, 618–623.
28 Yan LX, Liu YH, Xiang JW, Wu QN, Xu LB, Luo XL, Zhu XL, Liu C, Xu FP, Luo DL *et al.* (2016) PIK3R1 targeting by miR-21 suppresses tumor cell migration and invasion by reducing PI3K/AKT signaling and reversing EMT, and predicts clinical outcome of breast cancer. *Int J Oncol* **48**, 471–484.
29 Stagakis E, Bertsias G, Verginis P, Nakou M, Hatziapostolou M, Kritikos H, Iliopoulos D & Boumpas DT (2011) Identification of novel microRNA signatures linked to human lupus disease activity and pathogenesis: miR-21 regulates aberrant T cell responses through regulation of PDCD4 expression. *Ann Rheum Dis* **70**, 1496–1506.
30 Hu H, Li Y, Gu J, Zhu X, Dong D, Yao L, Lin C & Fei J (2010) Antisense oligonucleotide against miR-21 inhibits migration and induces apoptosis in leukemic K562 cells. *Leuk Lymphoma* **51**, 694–701.
31 Wickramasinghe NS, Manavalan TT, Dougherty SM, Riggs KA, Li Y & Klinge CM (2009) Estradiol downregulates miR-21 expression and increases miR-21 target gene expression in MCF-7 breast cancer cells. *Nucleic Acids Res* **37**, 2584–2595.
32 Yang CH, Pfeffer SR, Sims M, Yue J, Wang Y, Linga VG, Paulus E, Davidoff AM & Pfeffer LM (2015) The oncogenic microRNA-21 inhibits the tumor suppressive activity of FBXO11 to promote tumorigenesis. *J Biol Chem* **290**, 6037–6046.
33 Papagiannakopoulos T, Shapiro A & Kosik KS (2008) MicroRNA-21 targets a network of key tumor-suppressive pathways in glioblastoma cells. *Cancer Res* **68**, 8164–8172.
34 Gong B, Liu WW, Nie WJ, Li DF, Xie ZJ, Liu C, Liu YH, Mei P & Li ZJ (2015) MiR-21/RASA1 axis affects malignancy of colon cancer cells via RAS pathways. *World J Gastroenterol* **21**, 1488–1497.
35 Wang N, Zhang CQ, He JH, Duan XF, Wang YY, Ji X, Zang WQ, Li M, Ma YY, Wang T *et al.* (2013) MiR-21 down-regulation suppresses cell growth, invasion and induces cell apoptosis by targeting FASL, TIMP3, and RECK genes in esophageal carcinoma. *Dig Dis Sci* **58**, 1863–1870.
36 Liu M, Tang Q, Qiu M, Lang N, Li M, Zheng Y & Bi F (2011) MiR-21 targets tumor suppressor RhoB and regulates proliferation, invasion and apoptosis in colorectal cancer cells. *FEBS Lett* **585**, 2998–3005.